JOURNAL OF MATERIALS SCIENCE **38** (2003) 2049–2054

Nonlinear electrical characteristics and dielectric properties of (Ca, Ta)-doped TiO_2 ceramics

W. Y. WANG*, D. F. ZHANG, X. L. CHEN
Institute of Physics and Center for Condensed Matter Physics, Chinese Academy of Sciences, P.O. Box 603-49, Beijing 100080, People's Republic of China
E-mail: wangwanyan@yahoo.com.cn

TiO_2 ceramics doped with 1.0 mol% Ca and different concentrations of Ta were obtained by sintering processing at 1450°C. The microstructures, nonlinear electrical behavior and dielectric properties of the ceramics were investigated. The samples have nonlinear coefficients of $\alpha = 2.0$–5.0 and ultrahigh relative dielectric constants which is up to 10^5. Especially, the effects of Ta dopant on the nonlinear electrical characteristics and dielectric properties of the (Ca, Ta)-doped TiO_2 ceramics were studied in detail. When the concentration of Ta is 2.0 mol%, the sample exhibits the highest nonlinear coefficient and a comparatively lower dielectric constant. By analogy to a grain-boundary atomic defect model, the effects of Ta and the nonlinear electrical behavior of the TiO_2 system were explained.

1. Introduction

As it is known, many electronic circuits and systems are often used at special voltages and cannot withstand the overvoltage due to typical power system transients. Consequently, protective devices are needed to suppress the overvoltage for the electronic circuits and systems. Ceramic varistors are such devices. Up to now, they are the most commercial and effective protective devices because of the low cost and nonlinear current-voltage (I-V) characteristic, which makes them have the ability to sense and limit the overvoltage immediately.

SiC-based ceramic system was the earliest reported varistor [1]. Then ZnO-based varistors have been developed and widely used by virtue of their large nonlinear coefficients and other excellent property parameters [2, 3]. However, in recent years, other varistor systems are also under investigation in order to meet the new requirements of various applying fields, such as high capacitance, low breakdown voltage and multifunctional properties [4–6]. TiO_2-based ceramic system is one of the systems and has been widely studied [7–15] since Yan and Rhodes first reported that (Nb, Ba)-doped TiO_2 ceramics exhibited nonlinear I-V characteristic and could be used as a low voltage varistor [16]. Although various TiO_2 ceramics were reported in those papers, detailed study of (Ca, Ta)-doped TiO_2 ceramics has not been reported yet. The effects of Ta on the properties of the ceramics were not investigated, either. In this paper, the nonlinear electrical behavior and dielectric properties of (Ca, Ta)-doped TiO_2 ceramics were studied. In particular, the effects of Ta dopant on the nonlinear electrical behavior and dielectric properties of the ceramics were also investigated.

2. Experimental procedure

Appropriate amount of raw materials TiO_2 (99.99% purity), $CaCO_3$ (99.9% purity) and Ta_2O_5 (99.99% purity) were weighed according to the molar ratio of $Ca:Ta:Ti = 1:x:(99 - x)$, where $x = 0.5$, 1.0, 2.0 and 2.5. After being mixed and ground in alcohol, the powders were calcined in air at 1000°C for 12 h to fully decompose $CaCO_3$. Then they were granulated with 1 wt% polyvinyl alcohol binder and pressed at 200 MPa to form disks 10 mm in diameter and 1.5 mm in thickness. After being put into platinum crucibles and covered with Al_2O_3 lids, the disks were sintered in air at 1450°C for 1 h. The heating and cooling rates were 120°C/h and 150°C/h, respectively. After the temperature was decreased to 1000°C, the samples were allowed to cool naturally to room temperature.

To identify phases inside the sintered disks, the samples were characterized by a Mac Science M18AHF diffractometer with Cu K_α radiation. The microstructures of the samples were observed by a Hitachi S-4200 scanning electron microscope (SEM) with an Oxford energy-dispersive X-ray spectrometer. The grain sizes were determined by the intercept method. Apparent densities were measured by the Archimedes method.

For electrical measurements, both sides of samples were coated with a layer of silver conducting paint. The I-V characteristics were then measured using a stabilized electrical source (YJ 32-1) and two digital multimeters (HP 3468A, Solartron 7150). The frequency dependences of the sample capacitance (C), the dielectric loss ($\tan\delta$) and the resistivity (ρ) were determined on HP 4274A and 4275A LCR meters with a signal voltage of 0.5 V_{rms}. The measuring frequency range is from

* Author to whom all correspondence should be addressed.

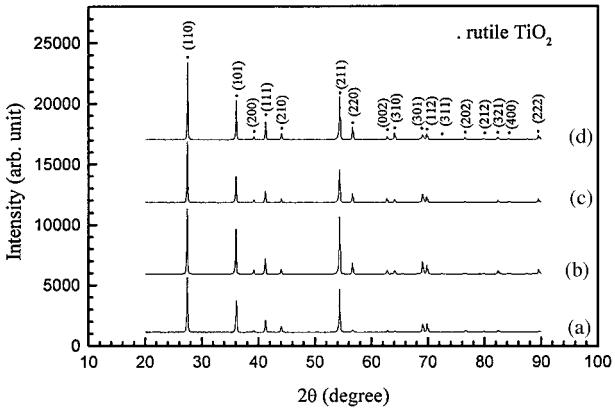

Figure 1 X-ray powder diffraction patterns for samples doped with 1.0 mol% Ca and different concentrations of Ta: (a) $x = 0.5$, (b) $x = 1.0$, (c) $x = 2.0$, and (d) $x = 2.5$.

200 Hz to 2 MHz. The impedance spectra measurements were performed at 150°C using an impedance analyzer (HP 4192A) with a 1.0 V a.c. signal in the frequency range from 5 Hz to 10 MHz.

3. Results and discussion

3.1. X-ray powder diffraction (XRD) analysis

The X-ray powder diffraction patterns of all samples are shown in Fig. 1. The analysis of the patterns indicates that no other phase except TiO_2 rutile phase exists in the samples. The rutile lattice constants of all samples are listed in Table I. From Table I, it can be seen that the rutile lattice constants increase monotonically with the Ta concentration. Therefore, all dopants of Ta were dissolved in the rutile lattice. CaO and Ta_2O_5 should form a solid solution in TiO_2 according to the following defect equations when the disks were sintered:

$$CaO \xrightarrow{TiO_2} Ca_{Ti}^{2-} + V_O^{2+} + O_O \quad (1)$$

$$Ta_2O_5 \xrightarrow{TiO_2} 2Ta_{Ti}^{+} + 2e^- + 4O_O + \frac{1}{2}O_2(g) \quad (2)$$

3.2. Microstructure

Fig. 2 shows SEM micrographs of all samples, illustrating that no apparent second phase appears in the samples. In addition, when $x = 0.5$, 2.0 and 2.5, respectively, the grains of each sample are relatively uniform in size. But when $x = 1.0$, the grains of the sample differ significantly in size. According to Table II, the average grain size of all samples falls in the range of 7.8–22.1 μm and the apparent relative densities are equal to or higher than 95%. For the sample with $x = 2.0$, the density is the highest.

TABLE I Lattice constants for samples doped with 1.0 mol% Ca and different concentrations of Ta

Ta (mol%)	a (Å)	c (Å)
0.5	4.5935	2.9598
1.0	4.5939	2.9606
2.0	4.5951	2.9632
2.5	4.5951	2.9636

3.3. Nonlinear electrical properties

Fig. 3 gives the I-V characteristics of samples doped with different concentrations of Ta. To scale the nonlinearity of samples, the nonlinear coefficient α was calculated according to the following equation:

$$\alpha = \frac{1}{\lg(V_2/V_1)} \quad (3)$$

where V_1 and V_2 are the voltages at 1 mA/cm^2 and 10 mA/cm^2, respectively. Table II lists the value of α as well as the breakdown voltage per grain boundary at 1 mA/cm^2 (E_{gb1}) of all samples. It can be seen that both α and E_{gb1} first go up with x increasing from 0.5 to 2.0, then go down with the further increment of x. When $x = 2.0$, the value of α is the highest and E_{gb1} is much larger than that of other samples.

Considering the potential barriers of TiO_2-based varistors are of Schottky type and the conduction mechanism in the ohmic region is by thermionic emission [17–19], the current density (J) is related to the electric field (E) and temperature (T) by the equation:

$$J = J_0 \exp[(\beta E^{1/2} - \phi_B)/kT] \quad (4)$$

where J_0 is a constant, ϕ_B is the interface voltage barrier height, k is the Boltzmann constant and β is a constant related to the barrier width of grain boundary (ω) by the relationship:

$$\beta \propto 1/[(r\omega)^{1/2}] \quad (5)$$

where r is the number of grains per unit length.

To calculate ϕ_B, Equation 4 is converted into the equation:

$$\ln J = \ln J_0 + (\beta E^{1/2} - \phi_B)/kT \quad (6)$$

Then the plots of $\ln J$ vs. $E^{1/2}$ were built up for all samples. By extrapolating the plots to $E = 0$, the intersection of the extrapolated line with the axis of $\ln J$ can be obtained for each sample (Fig. 4). Subsequently, the values of ϕ_B can be derived from the intersections and are presented in Table II. According to Table II, the value of ϕ_B increases with x when $x \leq 2.0$ and then decreases when $x > 2.0$.

In addition, as the slope of the $\ln J$ vs. $E^{1/2}$ plot gives β/kT, it is possible to obtain the value of β. By introducing the values of r and β into Equation 5, the relative magnitude of ω can be calculated, which is 0.113, 0.052, 0.286 and 0.316 when $x = 0.5$, 1.0, 2.0 and 2.5, respectively. According to these results, it can be seen that the value of ω varied with the increment of x.

3.4. Dielectric properties

Fig. 5 shows the relative dielectric constant (ε_r) vs. frequency (f) plot for samples doped with different concentrations of Ta. It can be seen that ε_r of all samples decreases monotonously with the increase of f. In the low frequency range (from 200 Hz to 1 KHz), the value

TABLE II Some characteristics of the samples doped with 1.0 mol% Ca and different concentrations of Ta

Ta (mol%)	d_r[a] (%)	d_g[b] (μm)	α	E_{gb1}[c] (V/g·b)	ϕ_B (eV)	ε_r (at 1 kHz)	tan δ (at 1 kHz)	ρ (kΩ·cm, at 1 kHz)
0.5	95.3	8.5	2.0	0.01	0.52	25271	0.10	631
1.0	97.0	22.1	2.4	0.03	0.53	61540	0.79	31
2.0	98.0	7.8	5.0	0.25	0.63	10255	0.45	392
2.5	95.0	9.4	2.0	0.02	0.51	55293	1.70	19

[a]Relative density (ratio of apparent density to the theoretical density of rutile, 4.25 g/cm^3).
[b]Average grain size.
[c]Breakdown voltage per grain boundary at 1 mA/cm^2.

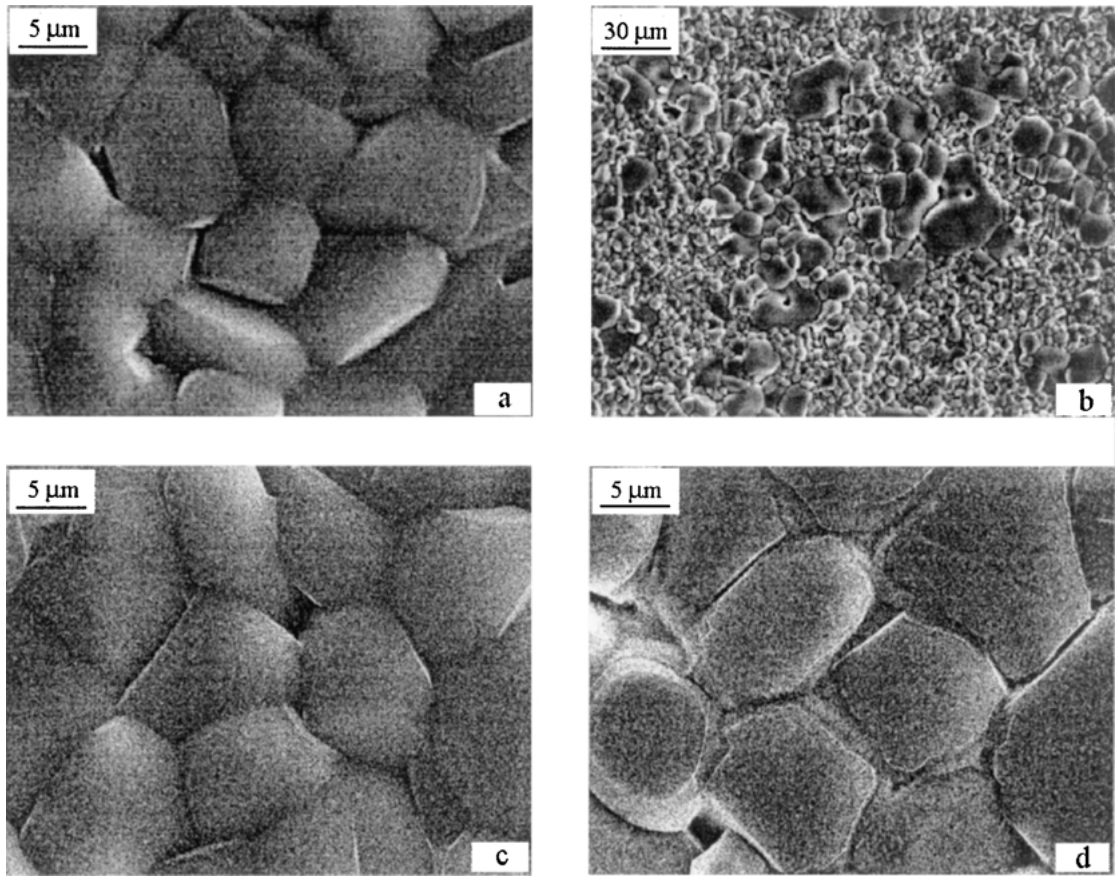

Figure 2 SEM micrographs of samples doped with 1.0 mol% Ca and different concentrations of Ta: (a) $x = 0.5$, (b) $x = 1.0$, (c) $x = 2.0$, and (d) $x = 2.5$.

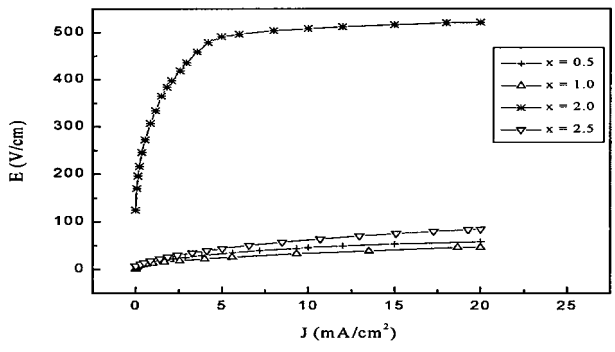

Figure 3 *I-V* characteristics of samples doped with 1.0 mol% Ca and different concentrations of Ta.

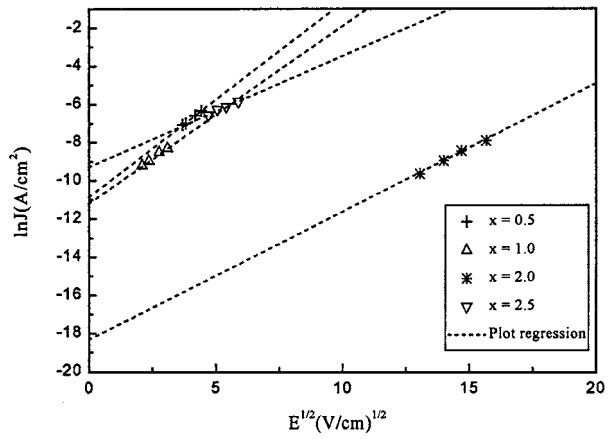

Figure 4 Ln J vs. $E^{1/2}$ plot for samples doped with 1.0 mol% Ca and different concentrations of Ta.

of ε_r of each sample is about or much larger than 10^4. Even at higher frequency (1 MHz), ε_r of each sample is still larger than 2×10^3. When $x = 1.0$ or 2.5, ε_r of both samples is much larger than that of other samples; when $x = 2.0$, ε_r is the lowest. Table II gives the value of ε_r at 1 KHz for each sample.

Fig. 6 illustrates the dielectric loss (tan δ) vs. frequency (f) plot for samples doped with different concentrations of Ta. For the sample with $x = 0.5$ or 2.0, tan δ is relatively low and a wide peak is observed

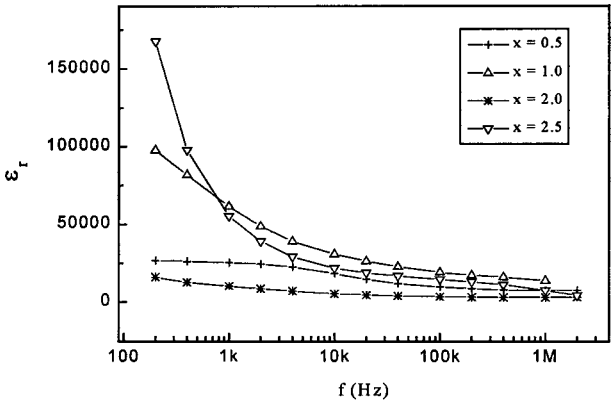

Figure 5 The relative dielectric constant vs. frequency plot for samples doped with 1.0 mol% Ca and different concentrations of Ta.

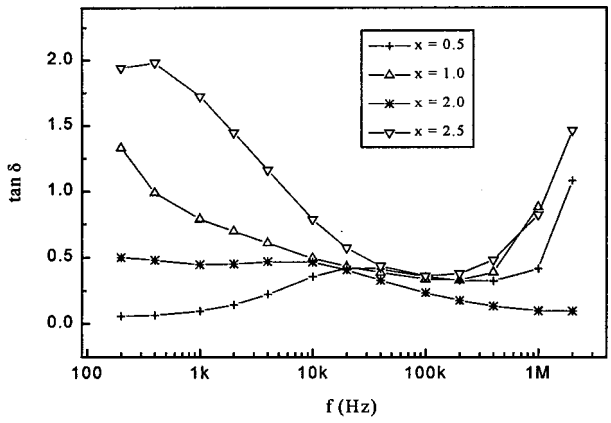

Figure 6 The dielectric loss vs. frequency plot for samples doped with 1.0 mol% Ca and different concentrations of Ta.

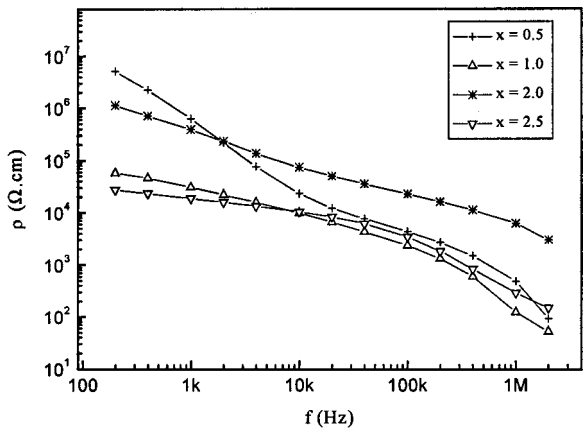

Figure 7 The resistivity vs. frequency plot for samples doped with 1.0 mol% Ca and different concentrations of Ta.

in each plot in the range of 1 KHz to 100 KHz. As $f > 100$ KHz, tan δ is the lowest for the sample with $x = 2.0$.

Fig. 7 shows the frequency dependences of the resistivity (ρ) of samples doped with different concentrations of Ta. It can be seen that the resistivity of each sample reduces monotonously with the frequency (f) increasing from 200 Hz to 2 MHz. In addition, the value of ρ keeps relatively higher in the whole measuring range of f for the sample with $x = 2.0$ while that of the sample with $x = 1.0$ or 2.5 is near or equal to the lowest value. The value of ρ of all samples at 1 KHz is also shown in Table II.

TABLE III Evaluated resistivities of grain boundaries and grain, ρ_{gb} and ρ_g, of the samples doped with 1.0 mol% Ca and different concentrations of Ta

Ta (mol%)	ρ_{gb} (kΩ·cm)	ρ_g (kΩ·cm)
0.5	521.95	1.56
1.0	11.85	0.77
2.0	722.51	-[a]
2.5	0.58	0.26

[a]Difficult to evaluate.

3.5. Impedance analysis

As the impedance plots of Z″ (reactance) versus Z′ (resistance) of samples measured at room temperature are quarter circles, it is difficult to distinguish the grain contributions from those of the grain boundaries. Therefore, the impedance spectra measurements were conducted at 150°C. The results are shown in Fig. 8. The numbers shown beside the arcs in the plots are the logarithmic exponents of measuring frequencies. It can be seen that there are two different arcs in Fig. 8a, b and d—a clear, larger one at lower frequencies (5–10^4 Hz) and an obscure, much smaller one at higher frequencies (10^4–10^7 Hz). The larger arcs are ascribed to grain boundaries and the smaller ones to grains. In Fig. 8c, only the larger arc is apparently seen while the smaller one seems disappeared. This is due to too small the grain contributions compared to those of the grain boundaries. From the diameters of smaller arcs and larger arcs, the resistivities of the grains and the grain boundaries, ρ_{gb} and ρ_g, were evaluated, respectively. From Table III, the sample with $x = 2.0$ possesses the highest grain boundary resistivity; then follows in the order the sample with $x = 0.5$, 1.0 and 2.5. In addition, for the samples with $x = 0.5$, 1.0 and 2.5, the grain resistivities decrease with the increasing doping concentration of Ta.

3.6. The grain boundary defect model

Gupta and Carlson developed a grain boundary defect model for ZnO varistors [20]. By an analogy to the model, the nonlinear behavior of (Ca, Ta)-doped TiO_2 ceramics can be explained. Fig. 9 shows the grain boundary defect model for the ceramics. Having an ionic radius very close to that of Ti^{4+} and a higher valence than Ti^{4+}, Ta^{5+} easily dissolves into the TiO_2 lattice and introduces the defects according to Equation 2. Due to the creation of electrons, Ta^{5+} decreases the resistivity of TiO_2 grains. At the same time, Ca^{2+} introduces the defects according to Equation 1 and prefers to segregate at the TiO_2 grain boundary. Therefore, there exist both the intrinsic TiO_2 defects (Ti_j^{4+}, V_{Ti}^{4-}, V_O^{2+}) and extrinsic defects (Ta_{Ti}^{+}, Ca_{Ti}^{2-}) at the grain boundaries. As shown in Fig. 9, the positive charges (Ti_j^{4+}, V_O^{2+}, Ta_{Ti}^{+}) are located on both sides of a grain boundary and the negative charges are distributed at the grain boundary interface. Due to the charge compensation between the positive charges and negative charges, a depletion layer is created at the grain boundary. As a result, a voltage barrier to the transport of the main charge carriers—electrons is formed and leads to the

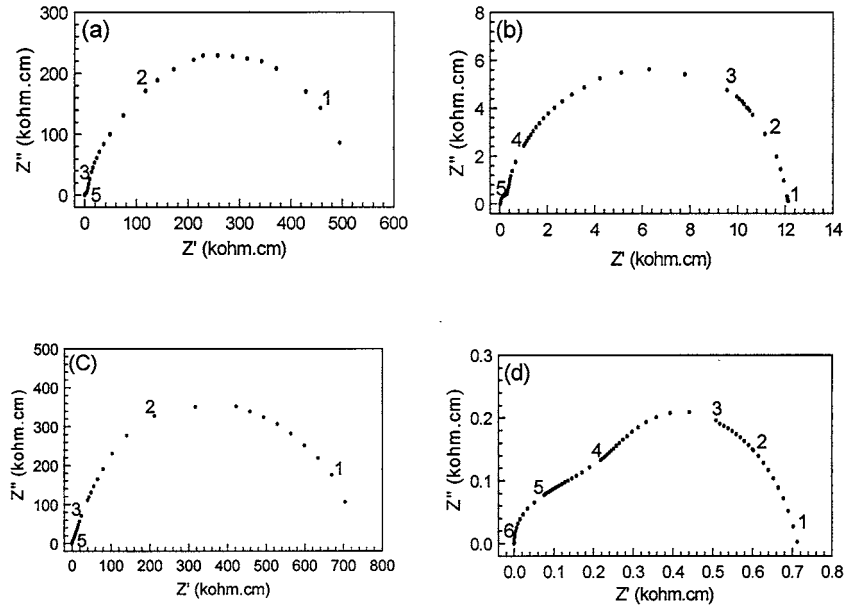

Figure 8 The complex impedance plots for samples doped with 1.0 mol% Ca and different concentrations of Ta: (a) $x = 0.5$, (b) $x = 1.0$, (c) $x = 2.0$, and (d) $x = 2.5$ (data taken at 150°C).

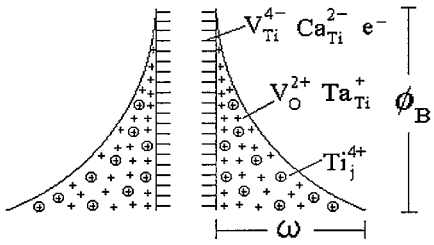

Figure 9 The grain boundary defect model for (Ca, Ta)-doped TiO_2 ceramics.

nonlinear electrical behavior of (Ca, Ta)-doped TiO_2 ceramics.

Based on the experimental results, there exist two effects of Ta on the nonlinear electrical behavior of (Ca, Ta)-doped TiO_2 ceramics. On the one hand, as Ta^{5+} dissolves into the TiO_2 lattice, the defect of Ta_{Ti}^{+} is introduced according to Equation 2 and located at the grain boundary. To maintain electrical neutrality, the positive charges (Ta_{Ti}^{+}) are compensated by negative charges. Consequently, the potential barrier is heightened due to the increase of the negative charges. The larger the doping concentration of Ta, the more the positive charges (Ta_{Ti}^{+}) and the more the negative compensating charges. As a result, the potential barrier is further heightened with the increasing x. Therefore, the nonlinearity of samples will be improved. On the other hand, the barrier width (ω) varies with the increment of x. When x goes up from 2.0 to 2.5, ω becomes larger and will influence the tunneling process of electron transport. Consequently, the nonlinearity will be worsened. Under the co-action of these two effects, there exists an optimal concentration of Ta for the electrical nonlinerity.

In addition, according to the grain boundary defect model, the nonlinear electrical property of varistors is related to the difference between the grain boundary resistivity (ρ_{gb}) and the grain resistivity (ρ_g). When the difference between the grain boundary resistivity (ρ_{gb}) and the grain resistivity (ρ_g) is great, an efficient boundary barrier layer will be formed to resist electronic conduction. Then the breakdown voltage (E_b) and the potential barrier (ϕ_B) are high and finally lead to the high nonlinear coefficient (α) of the varistor. From Table III, the sample with $x = 2.0$ possesses the greatest difference between the grain boundary resistivity (ρ_{gb}) and the grain resistivity (ρ_g). Therefore, when the doping concentration of Ta is 2 mol%, the sample has the highest nonlinear coefficient.

From Table II, it can be seen that the data of the dielectric constant, the dielectric loss and the resistivity do not have a systematic variation with the Ta concentration. A satisfactory explanation of these phenomena needs further work.

4. Conclusions

The Ta dopant has significant effects on the nonlinear electrical behavior and dielectric properties of (Ca, Ta)-doped TiO_2 ceramics. When the doping concentration of Ta increases from 0.5 to 2.5 mol%, the nonlinear coefficients of α of all samples is in the range of 2.0–5.0 and the relative dielectric constants are ultrahigh which is up to 10^5. In view of the nonlinearity, the optimal concentration of Ta is 2.0 mol%, which resulting in the highest nonlinear coefficient, higher resistivity and relatively lower dielectric constant with the smallest dielectric loss in high frequency range (100 KHz–2 MHz).

Acknowledgements

This work is financially supported by National Natural Science Foundation of China and Chinese Academy of Sciences. The authors would like to thank C. Y. Wang and T. S. Ning for their helps in SEM observation and XRD measurement, respectively.

References

1. H. F. DIENEL, *Bell Labs. Record* **32** (1954) 336.
2. L. M. LEVINSON and H. R. PHILIPP, *Amer. Ceram. Soc. Bull.* **65** (1986) 639.

3. T. K. GUPTA, *J. Amer. Ceram. Soc.* **73** (1990) 1817.
4. N. YAMAOKA, M. MASUYAMA and M. FUKUI, *Amer. Ceram. Soc. Bull.* **62** (1983) 698.
5. H. C. LING, M. F. YAN and W. W. RHODES, *J. Amer. Ceram. Soc.* **72** (1989) 1274.
6. Y. J. WANG, J. F. WANG, H. C. CHEN, W. L. ZHONG, P. L. ZHANG, H. M. DONG and L. Y. ZHAO, *J. Phys. D: Appl. Phys.* **33** (2000) 96.
7. J. M. WU and C. J. CHEN, *J. Mater. Sci.* **23** (1988) 4157.
8. C. J. CHEN and J. M. WU, *ibid.* **24** (1989) 2871.
9. J. M. WU and H. M. SUNG, *Mater. Sci. Eng.* B **3** (1989) 265.
10. J. PENNEWISS and B. HOFFMANN, *Mater. Lett.* **9** (1990) 219.
11. J. M. WU and C. H. LAI, *J. Amer. Ceram. Soc.* **74** (1991) 3112.
12. J. J. CHENG and J. M WU, *Jpn. J. Appl. Phys.* **35** (1996) 4704.
13. P. R. BUENO, E. CAMARGO, E. LONGO, E. R. LEITE, S. A PIANARO and J. A. VARELA, *J. Mater. Sci. Lett.* **15** (1996) 2048.
14. J. F. WANG, H. C. CHEN, X. H. ZHANG, D. J. ZHANG and W. L. ZHONG, *Chin. Phys. Lett.* **17** (2000) 530.
15. C. P. LI, J. F. WANG, Y. J. WANG, W. B. SU, H. C. CHEN and D. X. ZHUANG, *ibid.* **18** (2001) 674.
16. M. F. YAN and W. W. RHODES, *Appl. Phys. Lett.* **40** (1982) 536.
17. E. R. LEITE, J. A. VARELA and E. LONGO, *J. Mater. Sci.* **27** (1992) 5325.
18. S. A. PIANARO, P. R. BUENO, P. OLIVI, E. LONGO and J. A. VARELA, *J. Mater. Sci. Lett.* **16** (1997) 634.
19. Y. J. WANG, J. F. WANG, C. P. LI, C. CHEN, W. B. SU, W. L. ZHONG, P. L. ZHANG and L. Y. ZHAO, *ibid.* **20** (2001) 19.
20. T. K. GUPTA and W. G. CARLSON, *J. Mater. Sci.* **20** (1985) 3487.

Received 22 October 2001
and accepted 4 February 2003